*Journal of the European Ceramic Society* **14** (1994) 283–293

# Texture Formation in $Al_2O_3$ Substrates

A. Böcker, H. J. Bunge

Department of Physical Metallurgy, Technical University of Clausthal, Germany

J. Huber & W. Krahn

Hoechst CeramTec Selb, Germany

(Received 8 March 1994; accepted 13 April 1994)

***Abstract***

*The formation of textures (preferred crystal orientation) in $Al_2O_3$ substrates by green forming and subsequent sintering was studied. The observed texture type was always characterized by the basal plane parallel to the substrate plane. Crystal orientation within this plane was nearly axially symmetric. The c-axis pole distribution was obtained by an indirect method from several (hkil) pole distribution functions measured by X-ray diffraction.*

*Texture formation starts in the very first stages of green forming, the essential process being rigid particle rotation. Small texture changes were observed also in the initial stages of sintering. The strongest increase of texture, however, took place during grain coarsening at high sintering temperatures. The texture strength factor can be expressed quantitatively in terms of the green texture as well as the sintering time and temperature.*

*Die Texturentstehung in $Al_2O_3$ Substraten durch Grünformung und Sintern wurde untersucht. Die gefundenen Texturen waren charakterisiert durch die Vorzugsorientierung der Basisebene parallel zum Substrat. Innerhalb der Substratebene war die Kristallorientierung weitgehend achsialsymmetrisch. Die c-Achsenverteilung wurde röntgenographisch mit einem indirekten Verfahren aus mehreren Poldichteverteilungen (hkil) bestimmt.*

*Die Texturbildung beginnt in den allerersten Stadien der Grünformung durch starre Rotation der Partikel. Kleine Texturänderungen wurden auch in den Anfangsstadien der Sinterung beobachtet. Die stärkste Texturänderung trat jedoch während des Kornwachstums bei der Sinterung bei hohen Temperaturen auf. Es wird ein quantitativer Ausdruck für die Texturstärke in Abhängigkeit von der Grüntextur, der Sintertemperatur und der Sinterzeit gegeben.*

*On a étudié la formation de textures (orientations cristallographiques préférentielles) dans des substrats d'$Al_2O_3$ par formage du produit brut puis frittage. Dans tous les cas la texture est telle que le plan basal est parallèle au plan du substrat. L'orientation des cristaux dans ce plan était pratiquement symétrique autour de la normale du plan. On a obtenu la distribution des pôles correspondant à l'axe c par une méthode indirecte à partir de plusieurs fonctions de distribution des pôles (hkil) mesurées par diffraction X.*

*La formation d'une texture commence dès le début du formage du produit brut, le mécanisme essentiel étant la rotation en bloc des particules. On a aussi observé de petits changements de texture au début du frittage. Néanmoins, c'est lors de la croissance des grains à haute température que se produit le changement de texture le plus important. Le facteur de texture peut être exprimé quantitativement en fonction de la texture du brut, du temps de frittage et de la température.*

## 1 Introduction

Alumina substrates are used for many purposes, e.g. in the electronic industry. They have a polycrystalline structure consisting of crystallites of different orientation of their crystallographic axes. Many physical properties of $Al_2O_3$ are anisotropic. The macroscopic properties of the substrate are averages of the crystallite properties. They may thus also be anisotropic if the orientation distribution of the crystallites, i.e. the texture, is not random. The influence of texture on the macroscopic properties is different for different properties. The values of some properties may thus be improved, whilst others may be deteriorated by the presence of a particular texture. In either case, it is necessary to know the physical processes



*Journal of the European Ceramic Society* 0955-2219/94/$7.00 

underlying the development of a particular orientation distribution of the crystallites during the whole production process. Texture formation in $Al_2O_3$ substrates was studied by Dimarcello *et al.*[1] using X-ray pole figure measurements. Later on Nakada & Schock[2] stated that these were mainly surface textures. Since, in Ref. 3, an essential influence of the texture on physical properties was found, further investigations towards the texture formation mechanisms seemed desirable.

Alumina substrates are usually produced from powders by a green forming process followed by sintering. It was the purpose of the present investigation to study the influence of the process parameters on the final texture of the sintered substrates.

## 2 Texture measurement

The texture of a polycrystalline material is defined by the volume fraction of crystallites having a given orientation $g$ within an angular range $dg$ (see e.g. Ref. 4)

$$\frac{dV/V}{dg} = f(g) \qquad g = \{\varphi_1 \phi \varphi_2\} \tag{1}$$

The orientation $g$ of a crystallite is defined by its crystallographic coordinate system $K_B$ with respect to a sample coordinate system $K_A$ chosen in the substrate. It may be specified by three orientation angles, e.g. the Euler angles $\varphi_1 \phi \varphi_2$, as given in eqn (1). Texture measurement can be carried out by X-ray powder diffraction methods. Fixing the Bragg angle $\vartheta_{hkl}$ of a particular lattice plane and scanning the sample through two independent angles $\{\alpha\beta\}$ gives the pole density distribution (pole figure) of the normal direction to the reflecting lattice plane. A pole figure does not 'see' the third orientation angle of the crystallites, i.e. a rotation about this normal direction. The orientation distribution function (ODF) $f(g)$, eqn (1), can, however, be calculated mathematically from

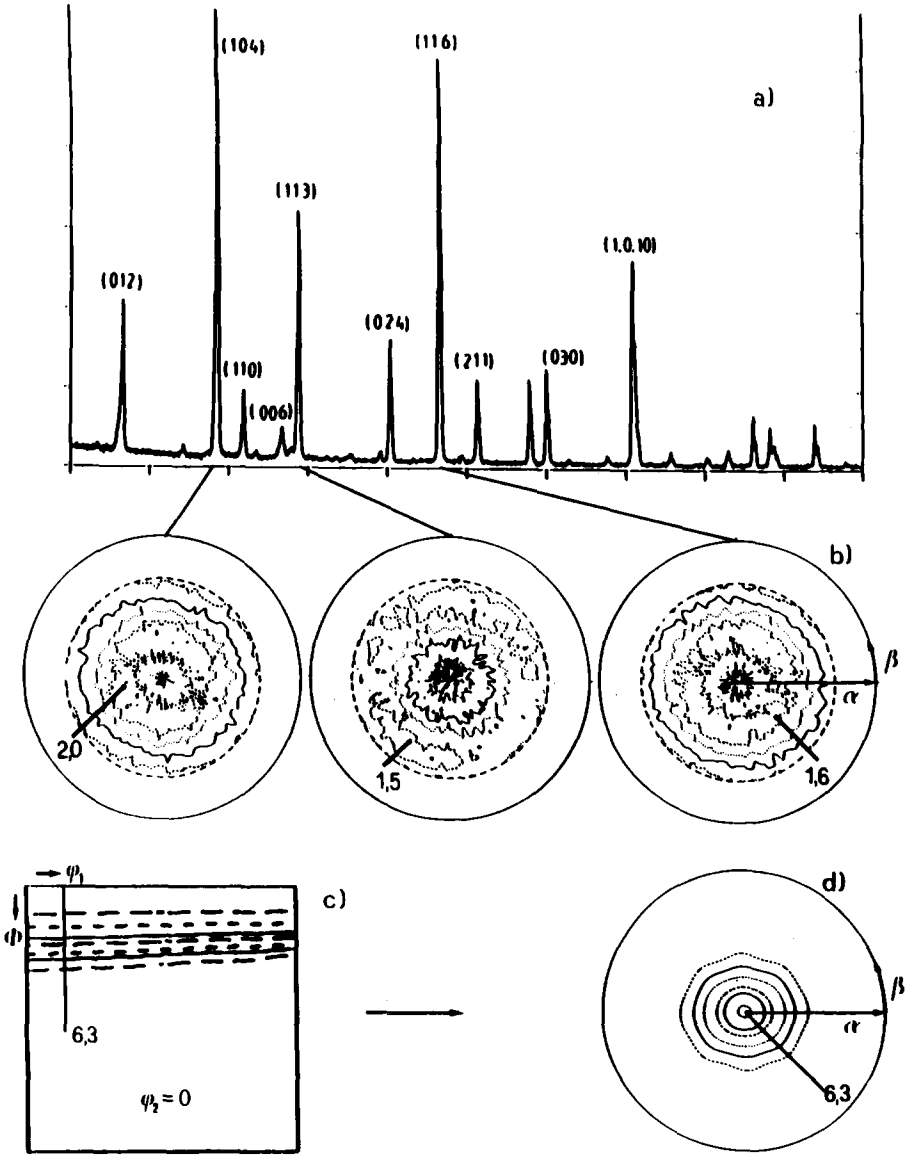


**Fig. 1.** Indirect determination of the basal plane pole figure in $Al_2O_3$ substrates (for details see Ref. 5): (a) diffraction diagram in sheet normal direction (indexed using the contracted three-index notation); (b) some pole figures of the high-intensity reflections; (c) orientation distribution function (section $\varphi_2 = 0$); (d) basal plane pole figure calculated from the ODF.

several pole figures. This can be achieved, for instance, by using a series expansion method. Vice versa, any pole figure can be 'recalculated' from the ODF. This is illustrated schematically in Fig. 1. Alumina, $\alpha$-$Al_2O_3$ (corundum), has a trigonal crystal structure (which has been treated here as being hexagonal for the purpose of texture analysis). In this case, the pole distribution of the crystallographic $c$-axes is particularly interesting. In fact, the texture of all substrates considered in this investigation could be completely characterized by the $c$-axis pole figure. The measurement of this pole figure is based on the (0006) basal plane reflexion. As is seen from Fig. 2, this reflection has sufficient reflectivity (structure factor) only in neutron diffraction, whereas for X-ray diffraction it is less than 1% of the strongest reflexion ($11\bar{2}3$).

Since neutron diffraction is more expensive than X-ray diffraction and can only be carried out at a research reactor, the indirect determination already described based on X-ray pole figures was used. Particularly, the pole figures ($10\bar{1}4$), ($02\bar{2}4$), ($11\bar{2}6$), ($11\bar{2}3$) were measured. These pole figures show rather 'diffuse' distributions so that they are not suitable for a direct estimation of the texture of the substrate (camouflaged texture). From these pole figures, the ODF and from that, in turn, the (0006) pole figure was calculated. This indirect determination of the (0006) pole figure was checked, in some cases, with direct measurement by neutron diffraction.[5] The deviation between the two methods was less than a few percent.

As is seen in Fig. 1, the (0006) pole figure has its maximum density in the substrate normal direction and the distribution is axially symmetric about this direction. This type of texture is completely characterized by a linear section through the (0006) pole figure, e.g. at $\beta = 0°$, as shown in Fig. 3. The shapes of all observed distribution functions were very similar. They could be well represented by Gaussian distributions as is also shown in Fig. 3. In this case the maximum pole density $P_{max}$ and the half-maximum width $b$ are related to each other, as shown in Fig. 4. The textures of the investigated substrates can thus be completely specified by either of these two quantities. In the following, the value $P_{max}$ which is, in this case, equal to the maximum orientation density $f_{max}$, is chosen.

The random distribution of crystallites is characterized by $f(g) = 1$. Hence, a 'texture strength factor' $\varphi$ is introduced:

$$\varphi = f(g)_{max} - 1 \qquad (2)$$

which is zero in the case of random orientation distribution.

It must be mentioned that in some cases small deviations from the axial symmetry of the texture were observed. These were, however, not taken into consideration in the present investigation.

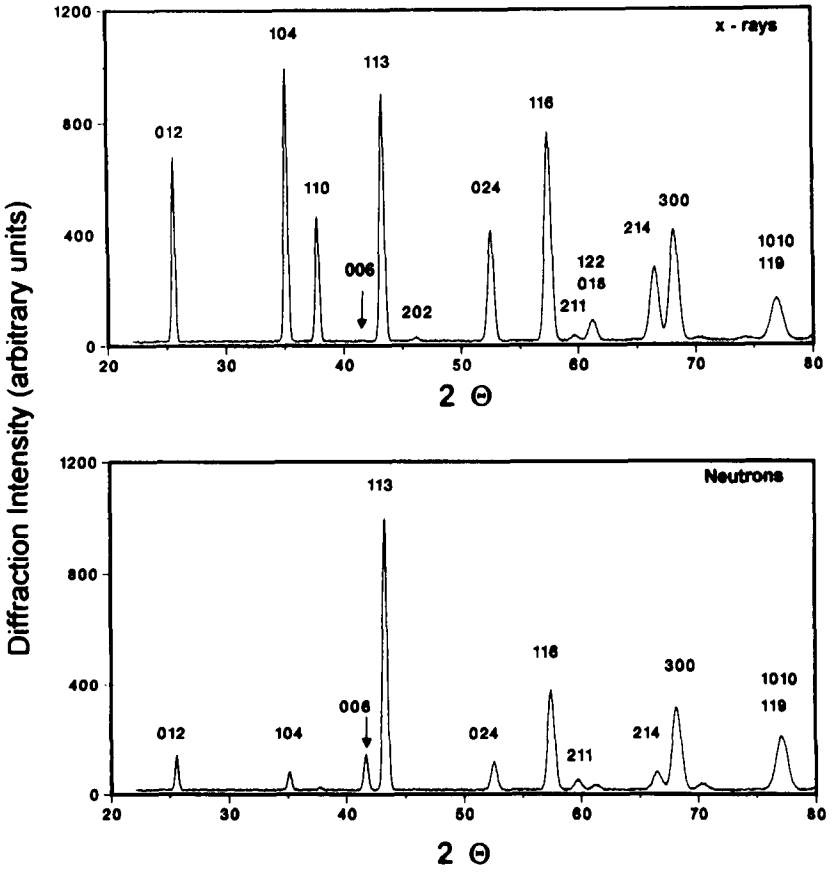


**Fig. 2.** Calculated diffraction diagrams of $Al_2O_3$ (random orientation distribution) (indexed in the three-index notation): (a) X-ray diffraction; (b) neutron diffraction.

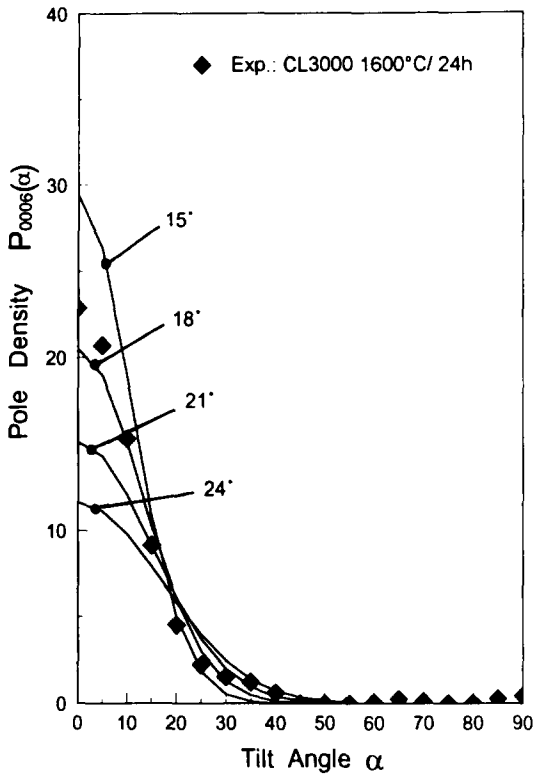


**Fig. 3.** (0006) pole figures (linear sections at $\beta = 0°$) calculated with Gaussian distribution of different spread widths, compared with experimental values of a sintered sample.

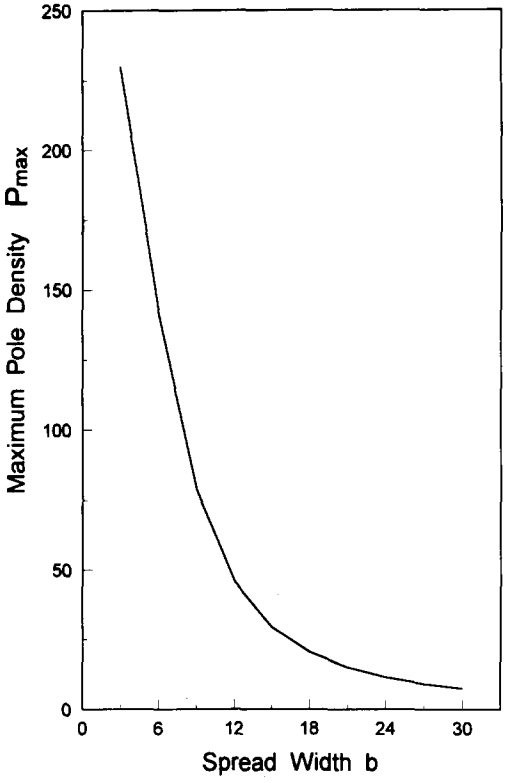


**Fig. 4.** Maximum pole density $P_{max}$ and half-maximum width $b$ for Gaussian distributions according to Fig. 3.

In order to interpret the texture measurements, the accuracy of the whole procedure must be known. The statistical error was estimated by repeating the pole figure measurement and ODF calculation ten times with the same substrate which was each time removed and again mounted in the sample holder. The results obtained deviated by no more than 2·5%, which is thus estimated to be the statistical error of the method (see Table 1).

The measuring conditions as well as the mathematical ODF calculation give rise to a certain broadening of the distribution function compared to the unknown 'true' function and hence to a decrease of the maximum orientation density. This is a systematic error which is difficult to estimate. By using several experimental conditions, a variation of about 8% was observed (see Table 1). An error of this magnitude must thus be admitted in the absolute pole density values. Under constant experimental conditions, as used in the following, this error may, however, be assumed to have been constant.

**Table 1. Reproducibility of the measured textures**

| | *Variation of texture strength (%)* |
|---|---|
| Reproducibility of texture strength in the same sample statistical error | ~2·5 |
| Estimated systematical error (with constant experimental conditions) | ~8·0 |
| Reproducibility within the same lot | ~5·0 |
| Through-thickness inhomogeneity | ≈14·0 |

## 3 Production of the Substrates

Starting materials for the production of substrates were alumina powders from different sources with different impurities and different particle size and shape distributions. These powders were milled using different types of mills, dry or with different liquid phases. Besides the individual charges, also various mixtures of these powders were used.

From the powders, 'green tapes' were produced in different ways, e.g. by dry calandering or from a slurry poured onto a moving steel band whereby the thickness of the layer could be controlled by a 'doctor blade'. The wet tape then moves through a drying furnace. The slurry contains an organic binder and plastifier which guarantees a sufficient strength and flexibility of the dried green tape, as well as certain sintering aids. Further parameters of this type of green forming are the band velocity and temperature profile in the drying furnace.

The second main step in the production process is sintering. Thereby various temperature regimes were used. Particularly, the substrates were heated up to the final temperature $T$, held there for a determined time $t$, and then cooled to room temperature. In this case, time and temperature are the main sintering parameters. A further param-

eter is the sintering atmosphere. In the present investigation it was air under normal pressure.

The texture strength of the final substrate must be assumed to be influenced by all production parameters. These parameters may vary to a certain unknown degree and so may the final texture. This influence was checked by measuring ten different substrates out of the same charge. The deviation was found in the order of 5% (see Table 1).

Finally, different charges run with nominally the same parameters were also compared. In this case, too, a deviation range of 5% was found (see Table 1).

## 4 Results

### 4.1 Texture homogeneity

In Table 1 the variation of the texture within one lot was found to be less than 5%. The samples measured in this case were taken from different positions along the length and width of the tape. Always the same side was, however, measured. Hence, the observed variation is an estimation of the planar homogeneity of the texture in the sintered substrate.

On the other hand, distinct through-thickness inhomogeneities up to 15% were observed. Since the final sintered substrate thus 'remembers' its upper and lower side during tape casting, this inhomogeneity must already be preformed in the green tapes.

### 4.2 Influence of the material and its preparation

In Section 3 several parameters which may influence the final texture in the substrate were mentioned. In principle, texture formation takes place during green forming as well as during sintering. During green forming, the powder particles themselves remain essentially undeformed. Texture formation will thus mainly be based on rigid particle rotation. This may depend, in turn, on the rotating forces exerted on the particles as well as on the ability of the particles to rotate. Hence, the size and shape distribution of the alumina particles the presence of other solid particles in the slurry, and the properties of the liquid phase may be the essential influencing parameters. Table 2 estimates the band width of texture strength in the green tape obtained by a variation of these parameters[6]. The size and shape distribution of the alumina particles will also influence the sintering process. The same holds, particularly, for the sintering aids, and also the binder is still present when sintering starts. Hence, these parameters may also modify the final texture after sintering even with equal green tape textures. Hence, Table 2 also gives band widths of sintered textures depending on the properties of the starting materials.

### 4.3 Texture formation during green tape casting

Texture formation during green tape casting is difficult to observe in the production line itself. The green tape textures given in Table 2 are those measured after the tapes have left the drying furnace. Hence, green forming of different slurries was studied in some manual tests. Figure 5 shows (0006) pole density curves of green tapes prepared by streaking the slurry onto the surface of a glass plate with a blade. This manual procedure was assumed to come nearest to the 'doctor blade' casting in the technological process. The third curve in Fig. 5 corresponds to a slurry which was just poured onto the glass plate without streaking its surface. It is seen that in this latter case the green texture was considerably weaker. The textures in Fig. 5 were measured after the tapes had dried sufficiently so that they could be prepared for X-ray measurement.

In order to detect possible texture changes during the drying process, the diffraction spectrum of several wet samples was determined during drying. This was done using a $\vartheta$–$\vartheta$ diffractometer (Siemens D500) which keeps the sample surface

**Table 2.** Band width of the green-forming parameters on the green and sintering textures

| | *Green texture* | | | *Sintering texture* | | |
|---|---|---|---|---|---|---|
| | *From* | *To* | *Band width* | *From* | *To* | *Band width* |
| Kind of raw alumina | 1·9 | 8·2 | 6·3 | 3·1 | 12·6 | 9·5 |
| Sintering aids | 4·6 | 6·2 | 1·6 | 8·6 | 10·1 | 1·5 |
| Binder | 6·3 | 7·0 | 0·7 | 10·5 | 11·5 | 1·0 |
| Solvent | 5·5 | 6·3 | 0·8 | 8·6 | 10·6 | 2·0 |
| Softener | 7·0 | 7·7 | 0·7 | 12·0 | 13·4 | 1·4 |
| Raw material processing | 5·0 | 5·4 | 0·4 | 10·4 | 14·1 | 3·7 |
| Slurry drying | 6·9 | 7·2 | 0·3 | 12·2 | 12·4 | 0·2 |
| Slurry caster | 4·6 | 5·2 | 0·6 | 8·8 | 9·9 | 1·1 |
| Tape thickness | 6·8 | 7·2 | 0·4 | 11·3 | 12·3 | 1·0 |
| Subsequent mechanical compaction | 6·3 | 6·7 | 0·4 | 9·4 | 10·0 | 0·6 |

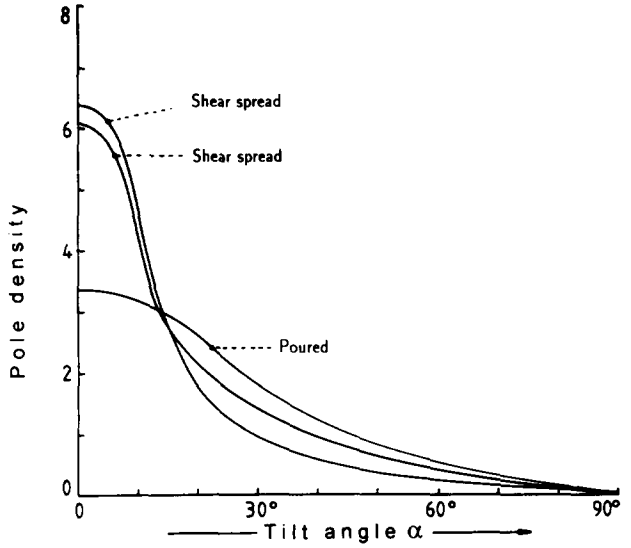


Fig. 5. (0006) pole density distributions of some manually prepared green tapes. Preparation was done either with or without streaking the slurry surface with a blade.

horizontal. In order to do the measurements as fast as possible a position sensitive detector was used which measures a selected part of the diffraction spectrum while being fixed in one position. The results are shown in Fig. 6. The intensity of the (0006) peak is measurable here, since it is stronger than in the case of random distribution. The measurement was started approximately 10 s after tape casting. Measurements were then taken in intervals of 18 s at first, later 1 min and 10 min.

It is seen that the texture strength remains virtually constant during the whole drying process. It was also observed that the slurry forms a 'skin' after a few seconds. After that, the texture has reached its final strength.

The texture of the skinless slurry was measured by covering the surface by a thin mylar foil which is completely transparent to X-rays. In this case the (0006) peak was virtually invisible in the diffraction spectrum. This confirms that texture formation takes place mainly during skin formation.

### 4.4 Texture evolution during sintering

Sintering was carried out using temperature schedules as shown in Fig. 7. It was found that the texture strength increases with sintering time as well as with sintering temperature. Figure 8 shows the typical time dependence at $T = 1600°C$. In this curve, two different ranges can be distinguished.

In the initial period the temperature rises up to its final value. During this period the organic material (solvent dispersant, plastifier and binder) is being burnt out and in the high-temperature range of this period, sintering already starts.

In the second period the texture strength increases steadily. During this period also the grain size increases steadily, as will be shown later.

The typical temperature dependence in relation to a dwell time of 2·5 h is shown in Fig. 9. Also in this curve, two different ranges can be distinguished. In the low temperature range the texture

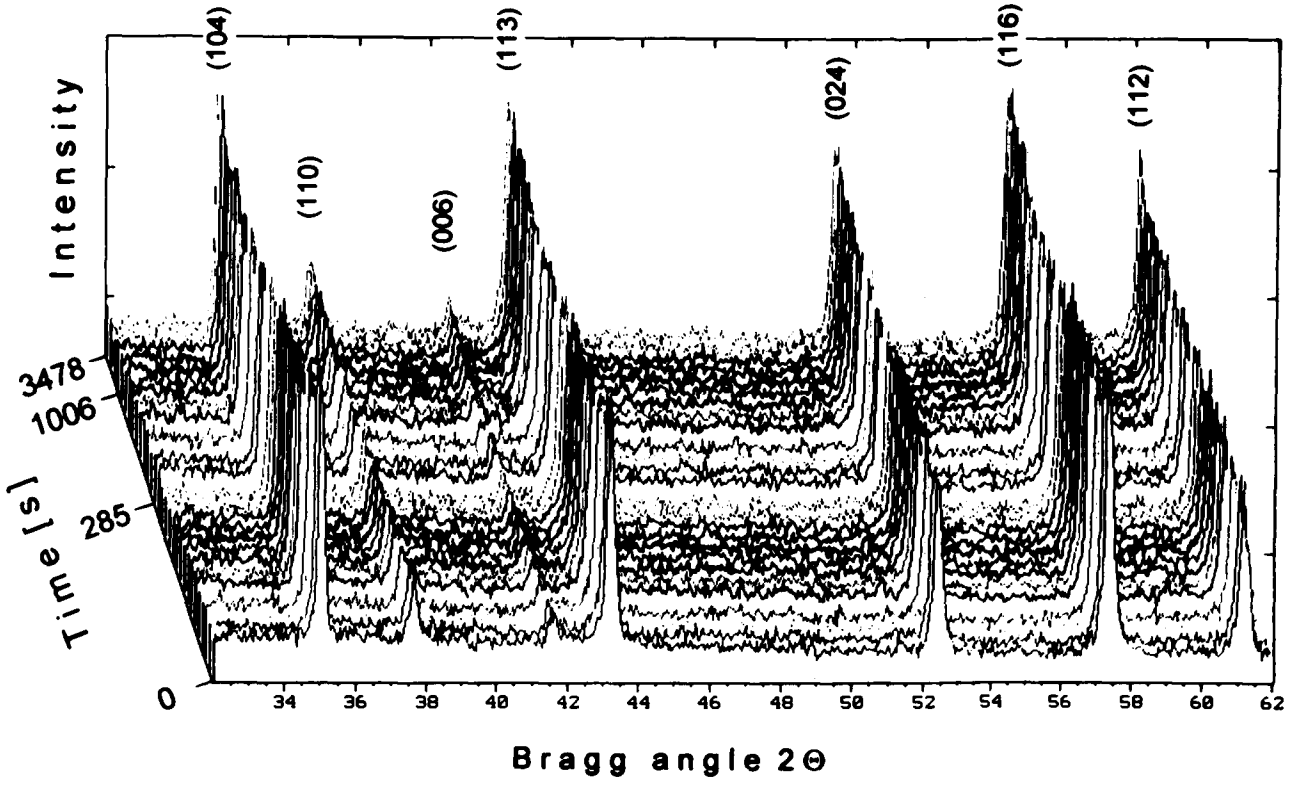


Fig. 6. Real-time diffraction spectra measured during drying of an $Al_2O_3$ slurry.

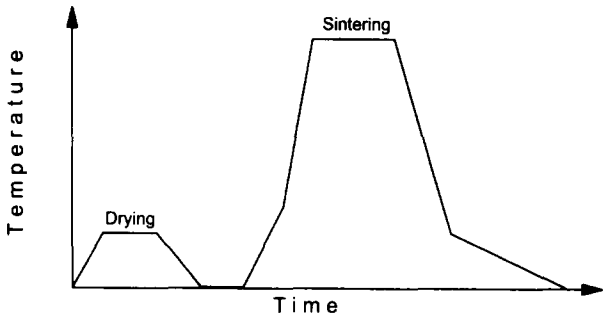


**Fig. 7.** Temperature schedule during sintering of $Al_2O_3$ substrates.

is only slightly stronger than the green texture. Nevertheless, it may be concluded that in many cases the small increase is significant.

In the high temperature range, the texture strength increases considerably with increasing sintering temperature. In this region very strong textures up to more than 30-times random could be observed.

### 4.5 Grain coarsening during sintering

For several materials the grain size at the beginning (0·5 h) and at the end (25 h) of sintering schedules as in Fig. 8 were measured. They are plotted in Fig. 10 together with the corresponding texture strengths.[7] It is seen that the green textures of these three samples are virtually identical and also the initial grain sizes are the same within the limits of experimental error. After sintering under (nominally) identical conditions both, grain size and texture have increased but to different extents. This shows that, on the one hand, grain coarsening is the essential factor relating the sintering texture to the green texture. On the other hand, neither the slopes of the three curves in Fig. 10 nor their endpoints are the same, indicating the presence of other influencing factors as will be discussed later in terms of eqn (7).

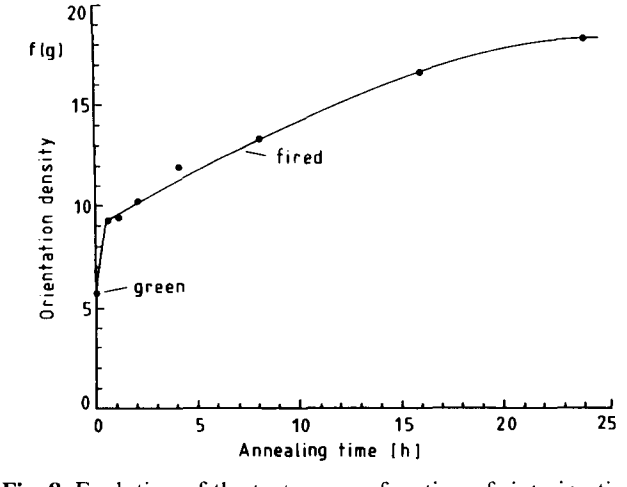


**Fig. 8.** Evolution of the texture as a function of sintering time at $T = 1600°C$.

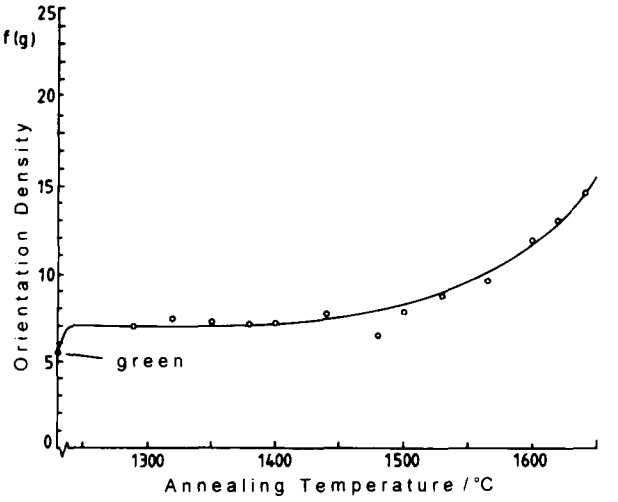


**Fig. 9.** Evolution of the texture as a function of sintering temperature after $t = 2·5$ h.

## 5 Discussion of the Results

The steps of texture formation that can be distinguished up to the final sintered state are summarized in Fig. 11:

- in the slurry, the $Al_2O_3$ particles probably have a random distribution.
- During tape casting a texture is being formed at the very beginning, particularly during skin formation. For this process, at least two different reasons may be assumed, namely:
  - —surface tension in the surface itself
  - —shear deformation of the near-surface region.
- After that first step, the texture remains virtually constant during further drying.
- A small texture strengthening takes place in the initial stages of heat treatment before grain growth.
- The strongest influence on the final texture is observed during final sintering. This increase

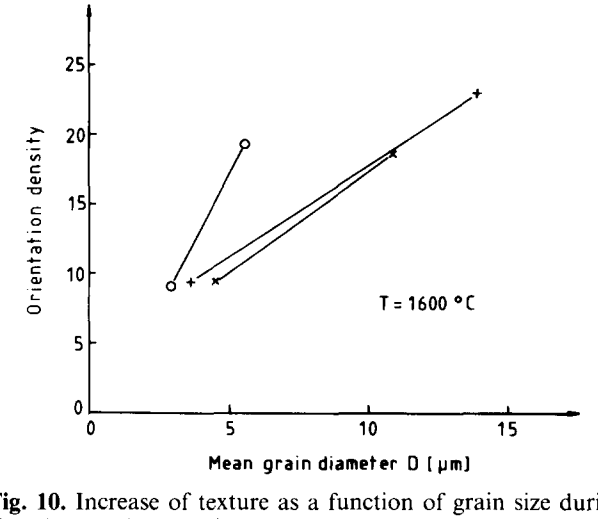


**Fig. 10.** Increase of texture as a function of grain size during sintering under nominally identical conditions. The three samples were taken from different charges.

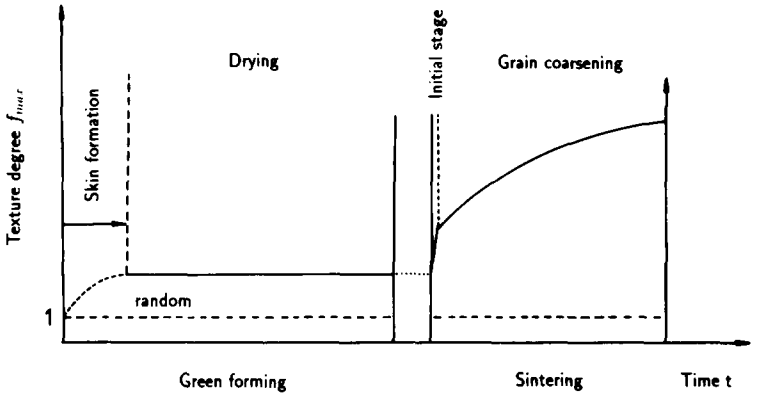


**Fig. 11.** Evolution of the texture during green forming and sintering of $Al_2O_3$ substrates.

of the texture strength may be attributed to grain coarsening.

The kinetics of grain coarsening have been studied experimentally by various authors and have been compared with model calculations. This process may be influenced by a number of parameters such as anisotropy of boundary energy as the driving force, anisotropy of boundary mobility, such that texture and texture changes may influence the growth kinetics. Furthermore, boundary pinning by solute atom concentration or by precipitates must be taken into consideration. In cases said to correspond to 'ideal' grain coarsening, a square root law was repeatedly found.

Assuming further, that texture development is the direct consequence of grain coarsening, the following expression for the time dependence of texture strength is tentatively assumed.

$$\varphi(t) = \varphi_0[1 + K \cdot \sqrt{t}] \qquad (3)$$

with $\varphi$ according to eqn (2). This relationship can be checked by plotting $\varphi/\varphi_0$ versus $\sqrt{t}$ as is done in Fig. 12. It is seen that eqn (3) may be considered as a reasonable approximation.

The growth rate factor $K$ must be assumed to depend on the temperature according to a Boltzmann factor. Hence, the time and temperature dependence may be summarized in the form

$$\varphi(T, t) = \varphi_0[1 + pm \exp -(Q/RT) \cdot \sqrt{t}] \qquad (4)$$

where $pm$ characterize the driving force and mobility for grain coarsening and $Q$ is the activation energy. The temperature dependence after a given sintering time follows from eqn (4)

$$\varphi(T) = \varphi_0[1 + C \exp -(Q/RT)] \qquad (5)$$

This relationship can be checked by plotting $\ln [\varphi(t)/\varphi_0 - 1]$ versus $1/T$ as is shown in Fig. 13. It is seen that the experimental results confirm this temperature dependence quite well.

Finally, it is assumed tentatively that the texture change at the beginning of the heat treatment, shown in Fig. 9, is zero in the case of random texture and increases with increasing texture. Then it can be taken into account by a factor $q$ additional to eqn (4). Hence, the final texture may be expressed in the form

$$\varphi^{substr} = \varphi^{green} q[1 + pm \exp -(Q/RT) \cdot \sqrt{t}] \qquad (6)$$

The driving force may be assumed to be proportional to the total grain boundary energy per unit volume at the beginning of grain growth. With a specific energy $\gamma$ per unit grain boundary area and assuming the initial total grain boundary area $a$ per unit volume, eqn (6) may then be brought into the final form

$$\varphi^{substr} = \varphi^{green} q[1 + a\gamma m \exp -(Q/RT) \cdot \sqrt{t}] \qquad (7)$$

With the sintering aids used, a liquid grain boundary phase is formed in the high temperature range. The growth process is then determined by the specific boundary energy $\gamma$, the mobility factor $m$ and the activation energy $Q$ of the system consisting of the grain boundary liquid and two liquid–solid interfaces (see Fig. 14). In spite of the non-crystallographic structure of the liquid phase, the interphase properties may, nevertheless, be crystallographically anisotropic. This has, however, not been taken into consideration in eqn (7). All three quantities $\gamma$, $m$, $Q$ will depend on the chemical composition which is mainly determined by the sintering aids used. According to the present results, the variation range of the activation energy

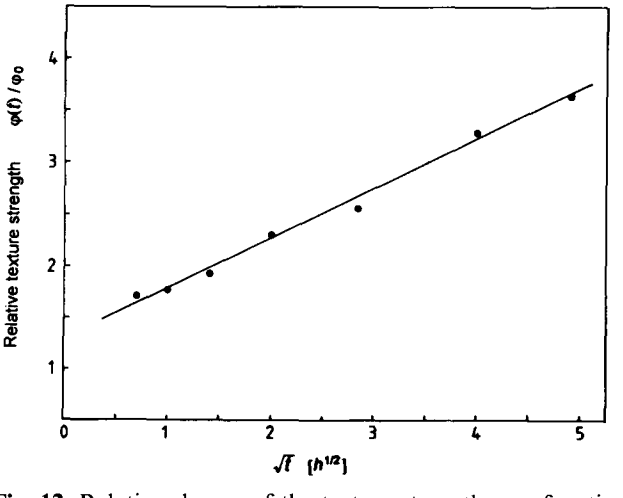


**Fig. 12.** Relative change of the texture strength as a function of the square root of sintering time at $T = 1600°C$.

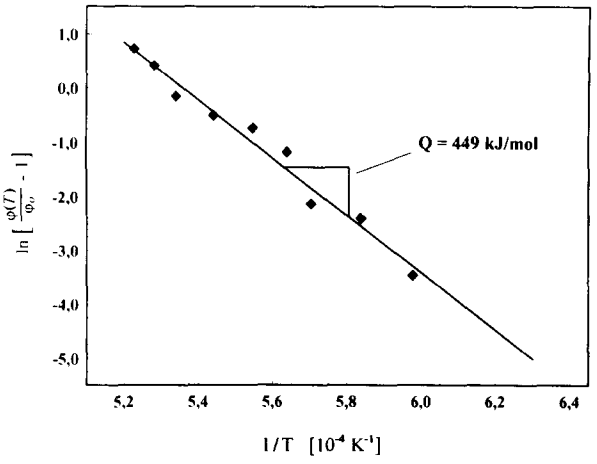


**Fig. 13.** Relative change of the texture strength as a function of the reciprocal sintering temperature after $t$ = 2·5 h.

was not very large. The same may be assumed for the factor $\gamma m$. The essential factor for grain growth is then the grain size distribution function $n(r)$. Assuming spherical grains the grain boundary area per unit volume is given by the expression

$$a = \frac{1}{6} \frac{\int r^2 n(r)\, dr}{\int r^3 n(r)\, dr} \tag{8}$$

This shows that the fine grain fraction of the powder contributes essentially to the driving force.

The factor $q$, i.e. the texture sharpening at the beginning of the heat treatment, was found to be near to unity. Hence, its influence on the final texture is not very strong. Texture changes in this range are not easy to understand. In the green foil, the $Al_2O_3$ particles have virtually not changed their original shape. During slurry casting the interspaces between them are filled with the solvent containing the polymer binder. During drying, most of the solvent is evaporated, leaving pores behind which contain a small amount of binder. During this stage, particle rotation may be possible. Its contribution to texture was, however, found to be rather small. In the first stages of heat treatment the binder burns off and the $Al_2O_3$ particles form solid-state grain boundaries. Thereby, surface tension may lead to particle rotation, which may have the observed small influence on the texture.

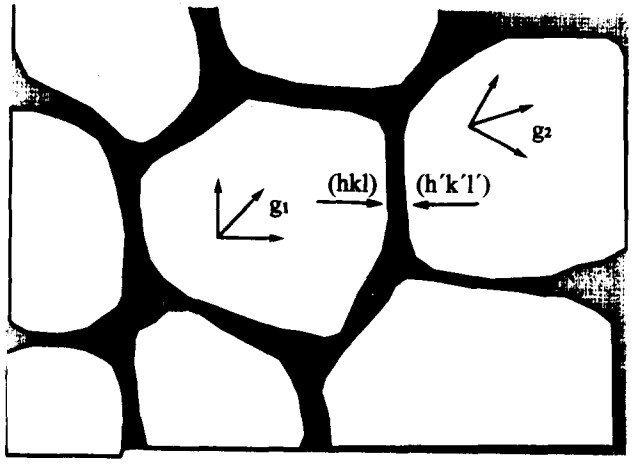


**Fig. 14.** Schematic representation of liquid-phase sintering.

The last remaining factor in eqn (7) is the green texture expressed by $\varphi^{green}$. In fact, this factor is very important for the final texture. It must be assumed that the green texture is formed by rigid rotation of particles having crystallographically oriented shapes. In the examples studied, the basal plane was preferentially oriented parallel to the substrate plane, i.e. parallel to the surface of the slurry and the green tape. Even if one assumes that the powder particles were agglomerated rather than being single crystals with well-developed faces, this shape effect may still prevail to a certain extent. Under these presumptions, it will be mainly the big particles which contribute to green texture formation. On the one hand, these particles may have the most pronounced crystallographic shapes and on the other they will experience the strongest rotational forces. It is thus assumed that the green texture is dominated by the big particles.

During grain growth, it is the big grains which grow on the expense of the small grains. If the big grains have a preferred orientation, then this orientation will be enhanced during grain growth. This is the reason why the factor in brackets in eqn (7) applies to the texture sharpness in a similar way as to grain size during grain coarsening.

The influence of crystal orientation $g$ and grain size $r$ on grain coarsening has been considered theoretically.[8] According to these considerations it is necessary to take a four-dimensional orientation–size distribution into account. In the particular situation considered here, mainly one orientation is important, i.e. the basal plane parallel to the substrate. It was further assumed that this orientation was preferred in the green texture due to a crystallographic grain shape factor. It should thus be possible to understand texture formation in $Al_2O_3$ substrates in terms of two particle parameters, i.e. grain size and grain shape, as is shown schematically in Fig. 15. In this diagram any powder is characterized by a two dimensional distribution function specifying the relative number of particles having the particle size $r$ and a crystallographic shape factor $s$. The big particles will form green texture components according to their respective grain shape factor. It may be assumed also that the small particles contribute green texture components according to their shape factor, although the correlation between shape factor and green texture is probably smaller for these particles.

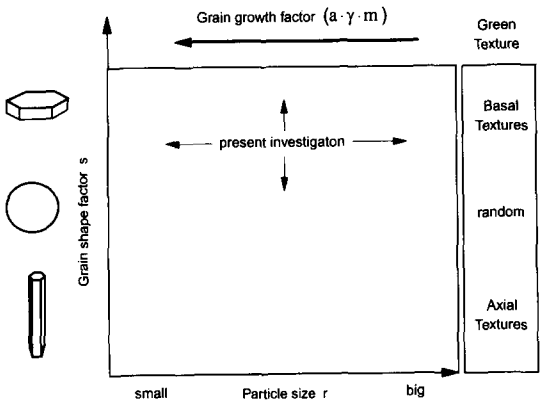


**Fig. 15.** Texture formation by green forming and sintering is influenced by the two-dimensional size–shape distribution.

In the second step, during sintering at sufficiently high temperatures, the big particles will grow on the expense of the small ones, thus extending their particular texture to the whole material.

In all samples investigated in the present study, the sintering texture was of the same type as the green texture, i.e. no new texture components emerged during sintering. Only the sharpness of the basal plane texture component increased. This experimental result is attributed, here, to the particular situation that the big particles were all 'plate-like' and hence developed a single-component texture during green forming. When using other types of powders containing big particles of other crystallographic aspects, this may no longer be true. Particularly, one may think of 'needle-shaped' particles with the needle axis being the crystallographic *c*-axis, e.g. $Al_2O_3$ whiskers. Particles of this shape will probably arrange themselves with the *c*-axis in the substrate plane. Two further subtypes may then be distinguished, i.e.

(a) the distribution of *c*-axis in the substrate plane is random or
(b) the *c*-axes also have a preferred orientation with respect to the flow direction during green forming.

Textures of this type may be called 'axial' textures as opposed to 'basal' textures as studied in the present investigation.

'Axial' textures of subtype (a) give rise to planar isotropy of the resulting materials, whereas those of subtype (b) may have planar anisotropy of their physical properties.

'Basal' textures, as they were found in the present investigation, were always very near to planar isotropy as already mentioned. (Although, in principle, also the *a*-axes may arrange themselves preferentially with respect to the flow direction.)

From Fig. 15 conclusions can be drawn as to how to obtain a particular texture in the final fired material. For a strong 'basal' or 'axial' texture a big particle fraction of 'plate' or 'needle' particles should be present. Besides this, a small particle fraction should also be present in order to accelerate grain growth.

In order to obtain a material with random texture several strategies can be thought of:

(1) The big particles should have no preferred crystallographic shape.
(2) If the powder contains big particles with either a 'plate' or a 'needle' shape, their, influence on the final texture may be compensated by adding big particles of the opposite shape. In this case, not really random distribution is to be expected but a 'mixed' texture containing basal as well as axial components compensating each other to some extent.
(3) Making the particle size distribution narrower, e.g. by using monosize powders, the grain growth factor should be reduced. In this case the final texture should be near to the green texture which was generally much weaker than the grain growth texture.

Finally, it may be concluded that the principles of texture formation described in Fig. 15 apply equally well also to other ceramic materials produced by green forming and subsequent sintering with grain growth.

## Acknowledgement

This work was sponsored by the Federal Minister of Research and Technology of Germany (BMFT).

## References

1. Dimarcello, F. V., Key, P. L. & Williams, J. C., Preferred orientation in $Al_2O_3$ substrates. *J. Am. Ceram. Soc.*, **55** (1972) 509–14.
2. Nakada, Y. & Schock, T. L., Surface texture formation in $Al_2O_3$ substrates. *J. Am. Ceram. Soc.*, **58** (1975) 409–12.
3. Klein, H., Waibel, B., Martin, W. & Bunge, H. J., Reliability of copper metallized $Al_2O_3$ substrates during thermal cycling as a consequence of preferred orientation (texture). In *Joining Ceramics, Glass and Metal.* ed. W. Kraft. DGM Informationsgesellschaft Oberursel, 1989, pp. 285–90.
4. Bunge, H. J., *Texture Analysis in Materials Science.* Butterworths Publ., London, 1982.
5. Böcker, A., Brokmeier, H. G. & Bunge, H. J., Determination of preferred orientation textures in $Al_2O_3$ ceramics. *J. Eur. Ceram. Soc.*, **8** (1991) 187–94.
6. Bunge, H. J., Böcker, A., Ernst, J. & Krahn, W., Einfluß von Material und Verarbeitung auf die Texturausbildung in $Al_2O_3$ Substraten. In *Proc. 2. Symp. Materialforschung*, Dresden, 1991. Bundesminster für Forschung und Technologie, pp. 1823–33.

7. Böcker, A., Bunge, H. J., Ernst, J. & Krahn, W., Texture evolution in $Al_2O_3$ sheets by grain growth during sintering. In *Recrystallization '92*, ed. M. Fuentes & J. Gil Sevillano. Trans Tech Publications, Switzerland, 1993, pp. 575–8.

8. Bunge, H. J. & Dahlem-Klein, E., Model calculations of grain growth by anisotropic boundary energy and mobility in textured materials. In *Recrystallization '92*. ed. M. Fuentes & J. Gil Sevillano. Trans. Tech. Publications, Switzerland, 1993, pp. 299–304.